Core-Shell Electrospun Polycrystalline ZnO Nanofibres for Ultra-Sensitive NO_2 Gas Sensing

Atif Aziz [a], Nikhil Tiwale [a], Stephen A. Hodge [b], Simon J. Attwood [a], Giorgio Divitini [c], and Mark E. Welland [a]*

a. Nanoscience Centre, Department of Engineering, University of Cambridge, CB3 0FF, UK.

b. Cambridge Graphene Centre, Department of Engineering, University of Cambridge, CB3 0FA, UK.

c. Department of Materials Science and Metallurgy, University of Cambridge, CB3 0FS, UK.

KEYWORDS: Electrospinning, ZnO nanofibres, NO_2 gas sensing, polycrystalline fibres

ABSTRACT: This paper discusses the growth of polycrystalline, self-supporting ZnO nanofibres which can detect nitrogen dioxide (NO_2) gas down to 1 part per billion (ppb), one of the smallest detection limits reported for NO_2 using ZnO. A new and innovative method has been developed for growing polycrystalline ZnO nanofibres. These nanofibres have been created using core-shell electrospinning of inorganic metal precursor zinc neodecanoate, where growth occurs at the core of the nanofibres. This process produces contamination-free, self-supporting, polycrystalline ZnO nanofibres of the average diameter and grain size 50 nm and 8 nm respectively, which are ideal for gas sensing applications. This process opens up an exciting opportunity for creating nanofibres from a variety of metal oxides, facilitating many new applications especially in the areas of sensors and wearable technologies.

INTRODUCTION

ZnO was discovered over one hundred years ago.[1] However, it was only during the end of the last century that ZnO received due attention, in particular, from the semiconductor community that was exploring materials to fabricate blue LEDs.[2] Although it ultimately lost the battle to gallium nitride (GaN) as a source of blue light, due to its excellent physical and chemical properties, ZnO is proving to be a very desirable material for a wide spectrum of applications including gas,[3] chemical and bio sensing,[4] photovoltaic devices,[5] UV detectors,[6] piezoelectric power generators and energy storage devices.[7] It is also very resistant to radiation damage and therefore a very useful material for space applications.[8] ZnO crystals are grown using chemical vapour deposition (CVD), pulsed laser deposition (PLD), sol-gel and hydrothermal processes.[9] Using these techniques, ZnO nanostructures have been created in many different shapes such as nanowires, nanospheres, nanohelices, nanorings and nanobelts.[10] Polycrystalline ZnO thin films have been created using the sol-gel method.[11] However, there have been no reports of self-supporting polycrystalline ZnO nanofibres. While many electronic applications where a high mobility is crucial require monocrystalline ZnO, polycrystalline ZnO is essential for gas sensing applications due to a large number of interfaces [5] and surface area.[12]

NO_2 is one of a very toxic polutent gases, which causes respiratory and heart problems.[13] In 2010, upto 5879 premature deaths in London were linked to NO_2 poisoning.[14] European Union regulations requires the NO_2 level in cities to be less than 200µg/m^3 (106.4 ppb) over 1 hour average and 40µg/m^3 (21.3ppb) averaged over the whole year. NO_2 is currently detected by chemiluminicence detectors which are big, heavy and not easily portable. ZnO nanofibre sensors can provide a very cheap and reliable alternative to existing technology. Due to a large surface area, low dimensional materials are commonly used for gas sensing applications. ZnO

nanowires[15], ZnO nanoparticles[16] and qunantum dots (QD) [17] have been used by various groups for sensing NO_2 gas. ZnO nanoparticles and QDs have been assembled into two dimensional sheets for making gas sensors. It has also been reported that the sensitivity of the ZnO gas sensor increases as the grain size is decreased.[18] The most efficient geometery which can harness the benefit of small grains is to organise the zero dimensional (0D) nanograins into one dimensional (1D) chains, so that the surface area is maximised and a transport sensing device can be fabricated. In this work, we have developed a process for making polycrystalline ZnO nanofibres which can be visulized as a 0D nanograins organised in the form a 1D nanofibre, and they indeed provide a very high sensitivity to NO_2 gas.

CORE-SHELL ELECTROSPINNING

Electrospinning is used for creating a network of nanofibres. However, one of the limitations of conventional electrospinning is that it requires polymer materials which must have a sufficiently high viscosity (>0.1 Pa-s) and molecular weight (thousands of g/mol) so that they can be stretched during the electrospinning process into nanofibres.[19] Therefore, most of the low molecular weight inorganic metal precursor solutions, for example zinc acetate (MW: 183.5 g/mol) and zinc neodecanoate (MW: 407.9 g/mol) cannot on their own be electrospun. When attempting to electrospin these molecules the jets exiting the electrospinner nozzle quickly disintegrate into droplets due to Rayleigh and electric field induced axisymmetric instabilities.[20] Precursor solutions are therefore normally mixed with polymers such as polyvinyl alcohol (PVA)[21] leading to organic contamination in the obtained fibres.[22]

Disintegration of non-polymeric materials into droplets during electrospinning can be avoided if axisymmetric instabilities are suppressed. Here, this is achieved by encapsulating the non-polymeric metal precursor solution into a polymer shell. To make it to work, both core

and shell materials must satisfy at least two conditions. Firstly, no chemical reaction must occur between the core and the shell solutions that might create new compounds and block the nozzle. Secondly, the two solutions should not be readily miscible. The core-shell process presented in this work creates nanofibres from a ZnO precursor solution with a PVA polymer used as an outer shell that can be completely decomposed during a calcination process, as confirmed by transmission electron microscopy (TEM). These calcined nanofibres do not disintegrate into powder but maintain a self-supporting fibres structure created during electrospinning. Nanofibres formation during electrospinning is very fast (typically tens of meters per second), therefore, the solutions have a very little time to mix together during co-spinning; furthermore, ZnO precursor used in this study is not miscible with polymers,[23] therefore creates contamination free ZnO nanofibres. Since NO_2 gas molecules are known to adsorb near metal oxide grain boundaries, polycrystalline ZnO nanofibres are an ideal candidate for gas sensing applications. As a proof of concept, NO_2 chemiresistive gas sensing is performed using the ZnO nanofibres. NO_2 has been detected using ZnO nanowires/nanorods,[24] nanoparticles,[16] quantum dots,[17] and plasma sprayed ZnO coating.[25] ZnO nanofibres created using core-shell ES provide a very competitive approach for detecting NO_2 gas. This process is very scalable and can produce ZnO nanofibres over a very large area of many square meters. Ease of fabrication, scalability, and a very high sensitivity give these nanofibre sensors an advantage over the above mentioned competing technologies.

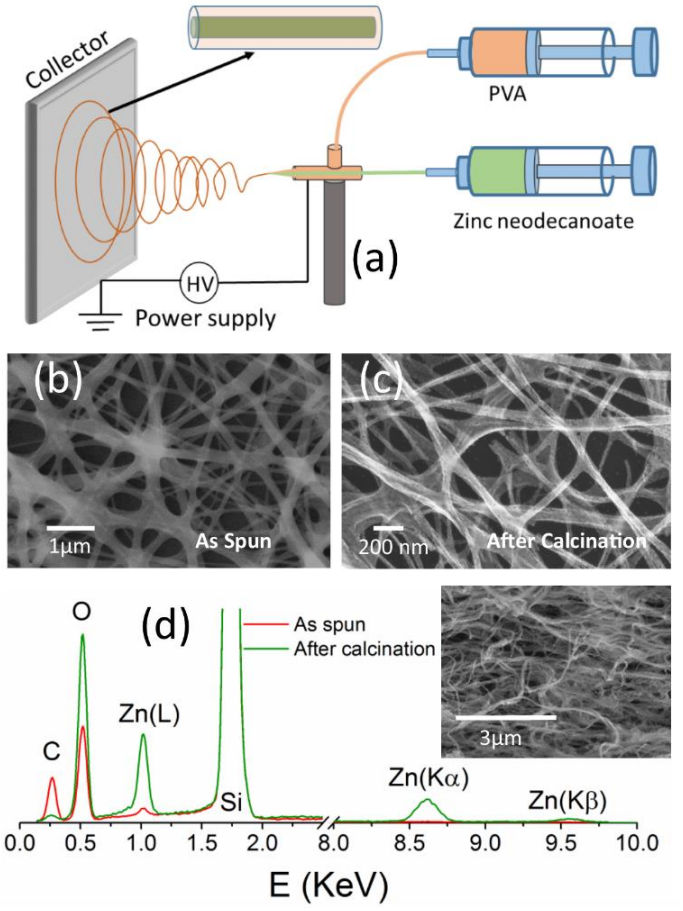

Figure 1. (a) A cartoon of the experimental setup of the core-shell electrospinning process. (b) SEM image of the as spun core-shell nanofibres. (c) SEM image of the fibres after calcination at 500°C in air. (d) A comparison of the EDX of the ZnO nanofibres after calcination and as spun fibres. Inset shows the area where the spectra is obtained.

Figure 1a shows a diagram of the basic setup used for creating the core-shell nanofibres. Custom made coaxial needles are used for simultaneously injecting two solutions for co-electrospinning. Zinc neodecanoate ($C_{20}H_{38}O_4Zn$), which is a Zn precursor solution, is injected through the inner needle. A PVA solution which forms the shell is injected through the outer needle. Zinc neodecanoate is used because it is a non-aqueous based precursor that does not dissolve PVA and is easily decomposed into ZnO in air.[26] No vacuum, gaseous atmosphere or pre/post treatment is required. The Zn precursor solution was prepared by mixing 4 parts by volume (80 %) zinc neodecanoate and 1 part by volume (20%) toluene. The shell polymer solution was made by dissolving 12 wt. % PVA in deionized (DI) water. Viscosities of the 80%

zinc neodecanoate and 12 wt % PVA solutions, at the shear rate of 100 s^{-1}, were $2.6x10^{-3}$ Pa s and 0.31 Pa s respectively.

Both the PVA and Zn precursor solutions were loaded into plastic syringes. For improving flow control, syringes were than loaded into mechanical dispensers. Flow rates of 5 µL/min and 6 µL/min were used for zinc neodecanoate and PVA, respectively. A high-voltage low-current DC power supply was used for creating a large electric field between a flat aluminium ground plate and the coaxial syringe needles. Figure S-2 shows the assembly of the coaxial syringe, including the inner needle (gauge 22) and the outer needle (gauge 18). The distance between the end of the needle and the ground plate was maintained at 15 cm and fibres were spun at 15 keV. Having spun the fibres on an aluminium electrode, fibres were peeled off and transferred onto a Si/SiO_2 (300 nm oxide layer) wafer and calcined in a tube furnace in air. One end of the tube was left open, while the other end was connected to an in-house exhaust so that air could flow through. The furnace was ramped up to 500°C at a rate of 10°C/min, maintained at 500°C for one hour and left to cool to room temperature before removing the sample. An 80% zinc neodecanoate sample provided the maximum density of fibres after calcination. Both 25% and 50% zinc neodecanoate in toluene were also spun but only a small number of fibres were present after calcination at 500°C. Fibres obtained from 80% zinc neodecanoate samples were used for further analysis and gas sensing.

ZnO NANOFIBRES

Figure 1b and 1c show scanning electron microscopy (SEM) images of the nanofibres before and after calcination at 500°C respectively. As-spun fibres readily charge while imaging in the SEM (due to the insulating organic layer), however, after calcination the nanowires do not charge during SEM imaging. Initial indication of the presence of ZnO was obtained by

performing the energy dispersive X-ray (EDX) spectroscopy measurements shown in figure 1d. EDX spectra reported are from as-spun and calcined fibres. For comparison, these spectra have been normalized to the intensity of the silicon peak present at 1.74 keV. The EDX spectrum of as-spun fibres shows very weak zinc peaks but a significantly stronger carbon signal. After calcination very strong Zinc Lα, Kα and Kβ peaks at 1.01eV, 8.64eV and 9.57eV emerge, as well as a significant increase in oxygen. On the other hand, the carbon peak is diminished. The silicon peak originates from the substrate. The oxygen signal is derived from both the SiO_2 substrate and the ZnO fibres.

Figure 2a to 2d show a series of SEM and TEM images of the ZnO nanofibres over a length scale varying from 10s of micrometers to a few nanometers. Figure 2a is an SEM image of a network of self-supporting ZnO nanofibres and the photoluminescence (PL) spectrum in Figure 2b is obtained from a similar fibres as shown in 2a. PL measurements were conducted with 266 nm laser wavelength operating at 2.06 mW power at room temperature. A small peak at 534 nm is the harmonic of the excited laser. A sharp peak at ~382 nm wavelength corresponds to the near band edge (NBE) emission of ZnO. The NBE emission has been attributed to free-exciton recombination within the ZnO matrix.[27,28] A broad deep-level emission within the 500-

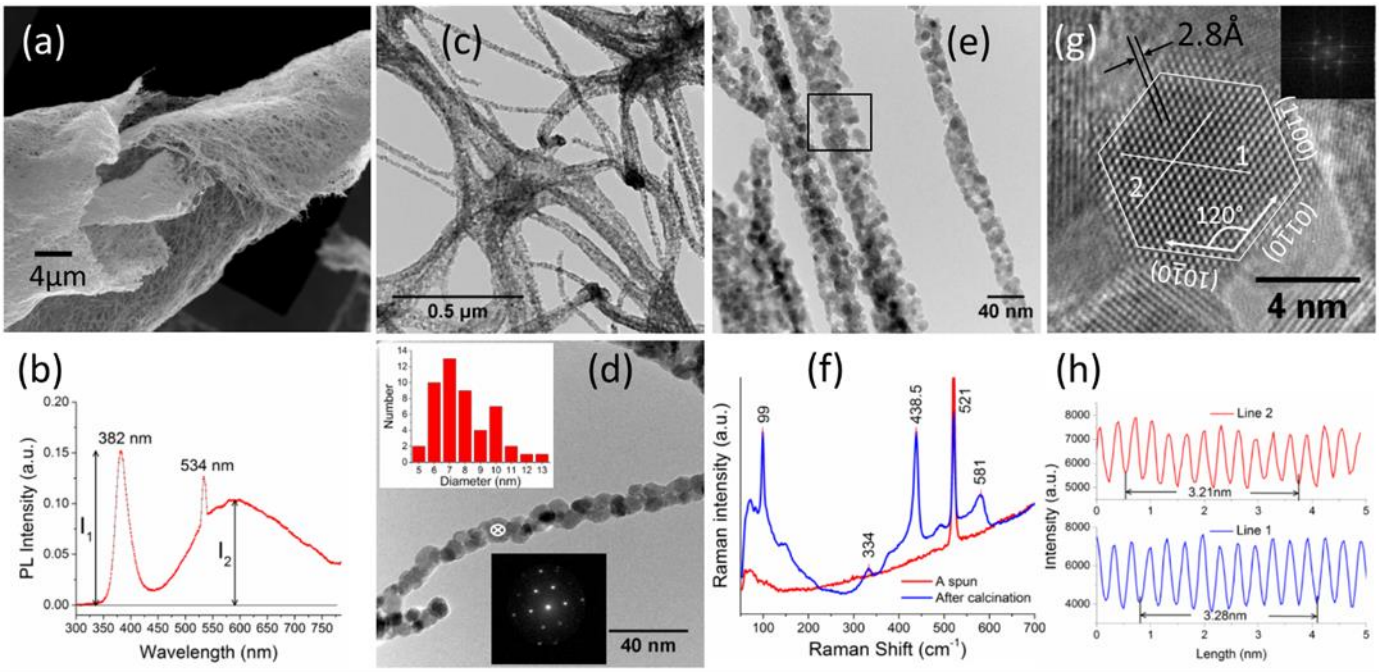

Figure 2. (a) SEM of of ZnO nanofibres after calcination. (b) PL spectra of the ZnO nanofibres. (c) TEM image of a collection of ZnO nanofibres. (d) TEM image of a single fibre. Top left inset is the histogram of the diameters of the grains of the nanofibre. Bottom inset is the diffraction pattern obtained from a single grain. (e) TEM image of ZnO nanofibres, the zoomed in image of the region marked as a black box is shown in the supplementary information. (f) Raman spectroscopy measurements of as spun fibres and fibres after calcination at 500°C. (g) High resolution TEM image of a single grain of ZnO crystal. Inset shows the FFT of the pattern. (h) The intensity profiles along the lines 1 and 2 shown in (g).

700 nm range is also observed which can be attributed to non-stoichiometric defects in the ZnO phase. Kim et al. correlated oxygen vacancies as a possible source of deep-level emission.[29] Ahn et al. correlated the defect peak observed in ZnO nanowires with gas sensitivity; NO_2 molecules have enhanced adsorption energy on oxygen vacancies and larger charge transfer.[15] In our ZnO nanofibres, there are a large number of grain boundaries and therefore a considerable amount of disorder and oxygen vacancies which are responsible for a large defect-level green emission and can provide preferential adsorption sites for NO_2 molecules.

Figure 2c is a TEM image of a collection of nanofibres and Figure 2d is the TEM image of a single nanofibre. TEM demonstrates that a large number of grains, each of a few nanometers in size, assemble into long fibres resulting in a large area of exposed surfaces and interfaces compared to monocrystalline ZnO. This image shows that ZnO nanofibres of diameters down to 20 nm can be fabricated using this electrospinning method. The top left inset shows a

histogram of circular diameters of the grains of the nanowire. It shows that the diameter of the majority of the grains varies from 6 nm to 10 nm. The bottom inset in Figure 2d shows the diffraction pattern obtained using a scanning transmission electron microscope (STEM) probe on one of the representative ZnO nanocrystals. It clearly shows that the ZnO nanocrystal has a hexagonal Wurtzite structure which is the most stable phase of ZnO. No evidence of the cubic structure was found. Figure 2e shows a collection of ZnO nanowires. Although nanowires of a diameter as small as 20 nm are created, the majority of the nanowires had diameters ranging from 30 nm to 70 nm, and the average diameter is about 50nm, as also evident from Figure S-1. Figure S-3, shown in the supporting information, is a high resolution magnified view of the region from panel 2e, as indicated by a black box. It clearly shows that the nanowire consists of ZnO nanograins, with negligible residues left over from the decomposition of the PVA shell. However, there are many nano-sized pores present in these nanofibres. These nanopores can arise due to the zinc precursor, which leaves voids during decomposition.

Graphs shown in Figure 2f present a comparison between the Raman spectra obtained from as-spun and calcined nanofibres. Raman peaks are observed at 99, 438.5 and 581 cm^{-1}, which correspond to the first order Raman modes E_{2L} (which is associated with the vibrations of Zn sub-lattice), E_{2H} (which is associated with the vibrations of oxygen sub-lattice) and LO modes (A_1(LO) and E_1(LO)), respectively. The A_1(TO) mode is rather weak but observable at 380 cm^{-1}. A multi phonon scattering mode can also clearly be seen at 334 cm^{-1}. These Raman modes are well documented in the literature and are associated with the hexagonal ZnO (space group C_{6v}^4).[30] No corresponding modes are observed in the as-spun fibres, except a sharp peak at 521 cm^{-1}, which is due to the Si substrate.

Figure 2g is a high resolution TEM image of a single grain of ZnO. The inset is the fast Fourier transform (FFT) image of the grain, further confirming the hexagonal structure of the ZnO nanocrystals. The spacing between (1100) planes is measured as 0.28 nm. Graphs shown in Figure 2h are the intensity profiles along line 1 and line 2 shown in Figure 2g, it provides a direct measurement of the average lattice spacing, which is 3.25 Å.

For sensing applications, surfaces as well as interfaces play a very vital role. Therefore, over the last few years there has been an increased interest in creating polycrystalline metal oxides consisting of the smallest possible grains.[18] A small grain size provides more surface area for the molecules to be adsorbed and therefore more sensitivity. The polycrystalline ZnO nanofibres presented here consist of one of the smallest nano grains reported in the literature,[28] with an average diameter of 8 nm and a narrow size distribution (5 nm to 15 nm). Furthermore, due to the pores present in the nanowires, interfaces are easily accessible to the gas molecules. In comparison, thermal radiation and precipitation methods have created ZnO grains of size varying from 60 nm to 500 nm.[18] Sol-gel deposition techniques have been used for creating films which consist of grain sizes varying from 13 nm to 22 nm,[31] and spray pyrolysis can create films containing grains of 8 to 32 nm.[28] These techniques are good for creating thin films but do not create nanofibres. The fabrication method presented in this paper combines the advantages of both small grain sizes as well as fibres of nanoscale dimensions.

NO_2 GAS SENSING

To test the NO_2 gas sensitivity of the synthesised ZnO nanofibres, a simple two terminal devices were fabricated. To fabricate ZnO transport devices, an as-spun ZnO nanofibres was placed on Gold/Titanium (Au (200nm)/ Ti (10 nm)) electrodes using a pair of tweezers. The entire chip, including the Au/Ti electrodes, was heated at 500°C in air. After calcination at 500°C, the ZnO fibres formed a network between the gold electrodes. A cartoon of the device

is drawn in Figure 3a, the gap between the electrodes A and B is 10µm and length is 100µm. Whereas, Figure 3b is an SEM image of the actual device showing the ZnO nanofibres between Au/Ti electrode. It also shows that the nanofibres are in good contact with the gold electrode. Some of the nanofibres are broken during the calcination process but the majority form a conductive percolating path between the gold electrodes.

Two terminal current-voltage (IV) curves were obtained at room temperature in an ambient air atmosphere and are shown in Figure 3c. A small non-linearity in the IV measurement performed in the dark is due to a Schottky contact between ZnO and higher work function of Au. UV light generates a large photo current as compared to the measurements performed in the dark and results in linear IV characteristics. Figure 3d shows the change in resistance of the ZnO nanofibre device when it is exposed to an atmosphere containing 25 ppb NO_2. Measurements are performed in the presence of a continuous UV LED light of wavelength 365 nm and at temperature 100°C. As shown in Figures S-5a and S-5b, sensitivity and the recovery of the signal improves as the temperature is increased. However, for practical applications the temperature should be kept as low as possible, mainly to reduce power consumption. Since 100°C is the boiling point of water, condensation and moisture do not build up on sensor. Therefore, we have chosen 100°C as an operating temperature. R_{air} is the resistance of the device in dry air just before introducing the NO_2 to the gas detection chamber. A constant voltage of 1 V was applied during the detection period. In the presence of 25 ppb NO_2, which flows at 500 sccm for 10 minutes, the change in resistance (ΔR) is about 0.26 MΩ (from 1.46 MΩ to 1.69 MΩ), $T1_{90}$= 178 s and $T2_{90}$= 374 s are the gas response and recovery times, respectively. $T1_{90}$ is the time taken for the resistance signal to reach 90% of the maximum change and $T2_{90}$ is the time taken for the resistance signal takes to recover back to 10% of the

starting value. From the change in resistance, the percentage response during 10 minutes of exposure to 25ppb NO_2 gas is 16%.

Depletion region controlled electron transport at the surface and grain boundaries is widely considered as a primary mechanism for gas sensing using ZnO.[32] NO_2 is an oxidizing gas, when NO_2 gas molecules are adsorbed on a ZnO nanofibre surface or a grain boundary, an electron is transferred from ZnO nanofibre to the NO_2 molecule and a surface depletion layer is formed, effectively changing the density and the mobility of electrons in the ZnO nanofibre. If the width of a ZnO nanofibre is comparable to the depletion region, the electron mobility and in return the resistance of the nanowire is greatly reduced. The Debye length, or charge screening length, which determines the width of a depletion region, is a characteristic length scale of a material. Debye length as function of carrier concentration at 100°C in ZnO is presented in the Figure S-7. If the dimension of a transport channel is close to the Debye length, its transport properties can easily be altered by the depletion region. In our sensor, ZnO grains have a size distribution from 5nm to 15nm, which is one of the smallest size reported in the literature and it is comparable to the Debye length in ZnO for a wide range of carrier concentration. The diameter of the fibres are also close to the Debye length. Therefore, nanofibres at this characteristic length scale have an excellent sensitivity to NO_2 gas. Furthermore, as compared to a single crystal ZnO nanowire, polycrystalline nanofibres have a large surface to volume ratio, therefore, even a very small quantity of NO_2 gas molecules adsorbed at the surface and interfaces can significantly reduce or even pinch off the electron channel.[16] When a ZnO sensor is exposed to a reducing gas like ammonia (NH_3) instead, NH_3 reacts with the adsorbed oxygen and electron are donated back to ZnO and the depletion region is reduced, in return decreasing its resistance. This behavior is also observed using our sensor, and a comparison between the

response of NO_2 and NH_3 is provided in a supporting information in Figure S-6, further validating the above mentioned sensing mechanism.

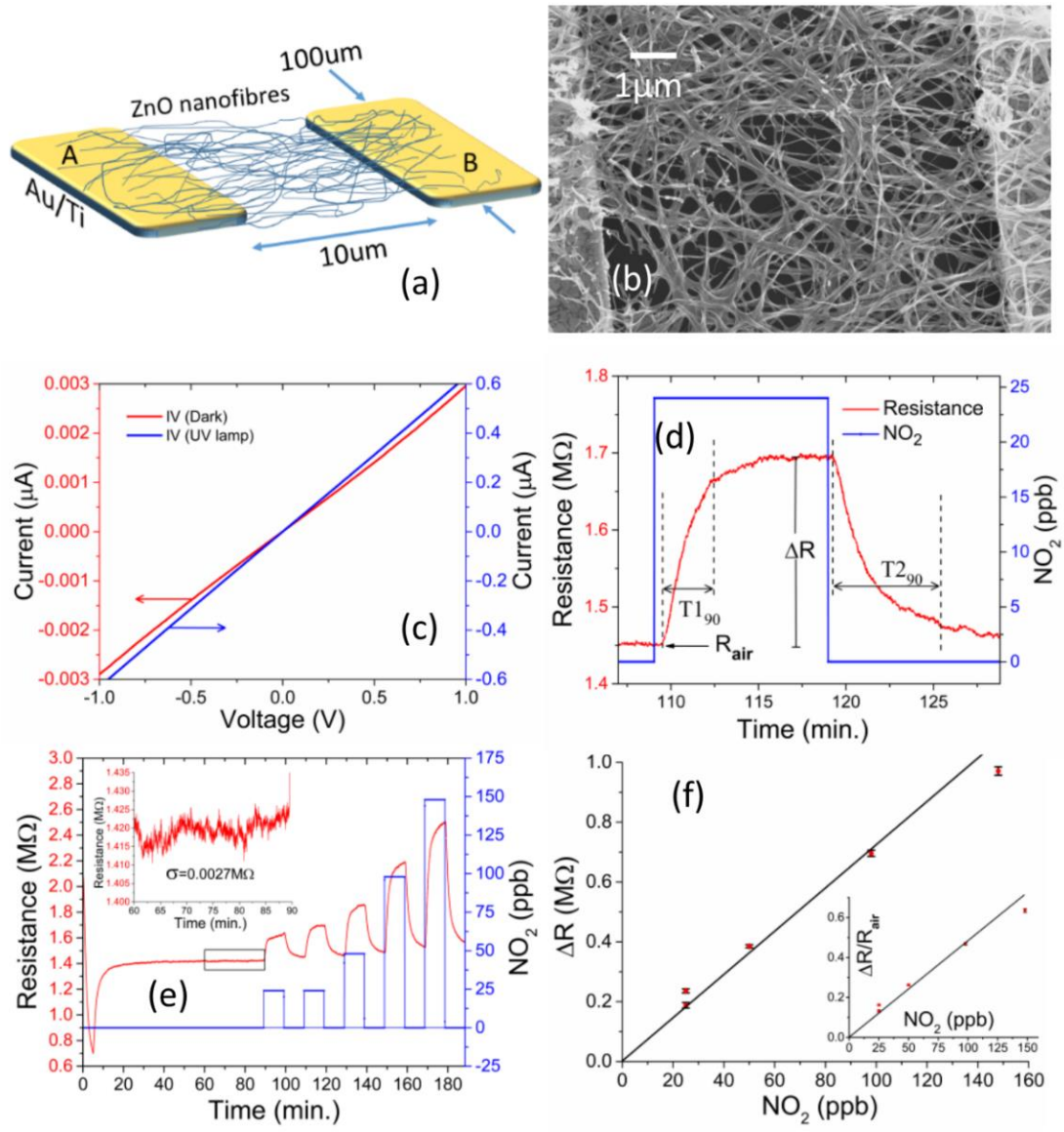

Figure 3: (a) A cartoon of the transport device used for detecting NO_2 gas. (b) SEM image of the ZnO nanofibres between the gold electrode of the device. (c) IV curves of the ZnO nanofibre device. Red curve is the measurement performed in dark. Whereas, blue curve is measured in the presence of a UV light of wavelength 254nm. (d) Blue curve is the NO_2 gas concentration. Red curve is the resistance of a ZnO device which changes in the presence of 25ppb NO_2 gas. (e) Change in resistance (red curve) of the ZnO nanofibres in the presence of the NO_2 gas (blue curve). Inset is the zoomed in region marked as a black box, which shows the noise level of the sensor in air. (f) Change in resistance verses concentration of NO_2 gas. Inset shows the sensitivity of the sensor.

Figure 3e shows the response of the ZnO device in the presence of 25 ppb, 50 ppb, 100 ppb and 150 ppb of NO_2 gas. From 0 to 5 minutes the device chamber is evacuated and the temperature is increased up to 100°C. From 5 to 90 minutes dry air is inserted into the chamber

and the pressure gradually reaches atm. pressure. Then, 25 ppb NO_2 gas is introduced to the chamber, which results in the change in resistance of the ZnO nanowires. Gas flow is maintained for 10 minutes, then NO_2 gas is turned off and replaced by dry air. Dry air flows for 10 minutes and the sensor is recovered. The process is repeated for 25, 50, 100 and 150 ppb of NO_2 concentrations. During this measurement the UV light remained on. Inset shows the standard deviation (σ) of the R_{air}, over a 30 min. period before the gas exposure, which is 2.7 kΩ. Figure 3f shows the change in resistance measured from the graph shown in 3e, as a function of NO_2 concentration. It is linear at low concentration and obeys Henry's ideal limiting law for low concentration[33] and has a slope (m) of 7.7 kΩ/ppb. Inset of Figure 3f shows the sensitivity ($\Delta R/R_{air}$) of the device which also shows a linear behavior at smaller concentrations. Similar results were obtained from another device which had a much lower density of fibres and a higher resistance, as shown in the Figure S-4. Using the change in resistance of the device subjected to NO_2 exposure and the standard deviation of R_{air}, one can estimate the lowest detection limit. From σ and m, the limit of detection (LOD=3σ/m) of the ZnO sensor is about 1 ppb and the limit of qualification, which is defined as LOQ=10σ/m, is 3.5 ppb. It clearly demonstrates that these ZnO nanofibres fabricated from the core-shell electrospinning method have a very good signal to noise ratio and high sensitivity to the NO_2 gas. Some additional measurements at high gas concentration are also presented in the supporting information (Figure S-5). Using improved device geometry such as interdigitated electrodes and aligned nanofibres, the lowest detection limit is expected to be further reduced to ppt (parts per trillion).

CONCLUSION

Non polymeric metal precursor solution are not electrospinable, however by choosing right materials and core-shell method Rayleigh instabilities can be suppressed and these precursor solutions can be electrospun. We have shown that polycrystalline self-supporting ZnO

nanofibres, containing nanograins of average diameter 8(±2) nm, can be created using core-shell electrospinning, which is a very cost effective and a scalable method. The proof of concept measurements presented in this paper suggest that these nanofibres provide a very promising route for creating highly sensitive NO_2 gas sensors. Using aligned electrospun fibres and interdigitated electrodes, the sensitivity of these devices could be increased further. The same fabrication principle can be applied to a number of other metal precursor solution, which can facilitate the creation of nanofibres of many other metal oxide materials. It is anticipated that the properties and functionalities of these new materials will greatly benefit the areas of sensing, energy storage and generation and wearable technologies. Due to the presence of nano grains, polycrystalline ZnO nanofibres may also find applications in spintronics where ferromagnetism in ZnO has been linked to the ZnO grain boundaries;[34] other applications may include purifying water, air and syngas..

Experimental section

Solution preparation

Zn precursor solution was prepared by mixing 4 parts by volume (80 %) zinc neodecanoate and 1 part by volume (20%) toluene. For complete dissolution, the solution was kept in ultrasound, at 80°C in a water bath, for 1 hour. After this, the solution was stable for more than a month. PVA solution was prepared using 65,000 MW PVA. A 12 wt% of PVA was gradually dissolved into a 90°C DI water and gently mixed using a magnetic stirrer for 1 hour. Viscosity of these solutions was measures at 25°C using TA instruments Discovery Hybrid Rheometer at a gap of 500µm. Since toluene dissolves rubber, plastic plunger syringe was used for the zinc neodecanoate solution.

Fabrication of devices

The Ti/Au contacts were fabricated using photolithography and a lift off process on a Si/SiO2 (300 nm) wafer; a 10 nm Ti layer and the successive 200 nm Au layer were deposited using an e-beam evaporator.

Characterization

Raman spectra were acquired at an excitation laser wavelength of 514 nm using a Renishaw InVia spectrometer with a 50x objective. The laser power was 1.5 mW. TEM images were obtained using a FEI Tecnai Osiris S/TEM working at 200 keV.

Gas sensing

Gas sensing experiments were performed using a Gas Sensor Testing System (Kenosistec, Italy). The system consists of mass flow controllers for dry air and nitrogen dioxide (NO_2), with a valve system to distribute gas mixture flow. Samples are placed inside an air-sealed chamber with 2 electrical probes contacting sample electrodes. Two probe resistance measurements are performed at a constant voltage of 1.0 V. Current is measured using a Keithley 6487 picoammeter. Prior to all experiments samples were exposed to vacuum ($\sim<5x10^{-5}$ bar) for 5 minutes. This is followed by exposure to dry air for 85 minutes to equilibrate the sensor to find the baseline resistance, R_{air}. A 1 ppm NO_2 in dry air cylinder was diluted further with dry air, which allowed the introduction of concentrations down to 25 ppb. Total gas flow rate was always maintained at 500 sccm. Sensing was performed by introducing incrementally increased NO_2 gas concentrations, holding at 10 minutes per concentration followed by 10 minutes of dry air to remove adsorbed NO_2 gas.

ASSOCIATED CONTENT

Supporting Information.

Size distribution of ZnO fibres, high resolution TEM image of ZnO fibres and some additional NO_2 gas sensing data at high gas concentration, humidity and higher temperature is also provided in the supporting information.

AUTHOR INFORMATION

Corresponding Author

* Dr Atif Aziz: aa267@cam.ac.uk

Author Contributions

The manuscript was written through contributions of all authors. All authors have given approval to the final version of the manuscript.

Funding Sources

Lloyd's Register Foundation, London, UK.

ACKNOWLEDGMENT

All the authors acknowledge the support of the Lloyd's Register Foundation, London, UK, who has funded this research through their grants to protect life and property by supporting engineering-related education, public engagement and the application of research.

REFERENCES

(1) Stone, G. C. Oxide of Zinc. *Trans. Am. Ins. Min. Metall. Eng.* **1917**, *57*, 682–695.

(2) Janotti, A.; Van de Walle, C. G. Fundamentals of Zinc Oxide as a Semiconductor. *Reports Prog. Phys.* **2009**, *72* (12), 126501.

(3) Zheng, Z. Q.; Yao, J. D.; Wang, B.; Yang, G. W. Light-Controlling, Flexible and Transparent Ethanol Gas Sensor Based on ZnO Nanoparticles for Wearable Devices. *Sci. Rep.* **2015**, *5* (June), 11070.

(4) Li, X.; Zhao, C.; Liu, X. A Paper-Based Microfluidic Biosensor Integrating Zinc Oxide Nanowires for Electrochemical Glucose Detection. *Microsystems Nanoeng.* **2015**, *1*, 15014.

(5) Hu, Q.; Li, Y.; Huang, F.; Zhang, Z.; Ding, K.; Wei, M.; Lin, Z. ZnO Nanowires Array Grown on Ga-Doped ZnO Single Crystal for Dye-Sensitized Solar Cells. *Sci. Rep.* **2015**, *5* (1), 11499.

(6) Alenezi, M. R.; Henley, S. J.; Silva, S. R. P. On-Chip Fabrication of High Performance Nanostructured ZnO UV Detectors. *Sci. Rep.* **2015**, *5* (1), 8516.

(7) Sun, H.; Zhang, Y.; Zhang, J.; Sun, X.; Peng, H. Energy Harvesting and Storage in 1D Devices. *Nat. Rev. Mater.* **2017**, *2*, 17023.

(8) Auret, F. D.; Goodman, S. A.; Hayes, M.; Legodi, M. J.; Van Laarhoven, H. A.; Look, D. C. Electrical Characterization of 1.8 MeV Proton-Bombarded ZnO. *Appl. Phys. Lett.* **2001**, *79* (19), 3074–3076.

(9) Kumar, R.; Al-Dossary, O.; Kumar, G.; Umar, A. Zinc Oxide Nanostructures for NO_2 Gas-Sensor Applications: A Review. *Nano-Micro Lett.* **2015**, *7* (2), 97–120.

(10) Wang, Z. L. Zinc Oxide Nanostructures: Growth, Properties and Applications. *J. Phys. Condens. Matter* **2004**, *16* (25), R829–R858.

(11) Znaidi, L. Sol-Gel-Deposited ZnO Thin Films: A Review. *Mater. Sci. Eng. B Solid-State Mater. Adv. Technol.* **2010**, *174* (1–3), 18–30.

(12) Tiwale, N. Zinc Oxide Nanowire Gas Sensors: Fabrication, Functionalisation and Devices. *Mater. Sci. Technol.* **2015**, *31* (14), 1681–1697.

(13) Hoek, G.; Krishnan, R. M.; Beelen, R.; Peters, A.; Ostro, B.; Brunekreef, B.; Kaufman, J. D. Long-Term Air Pollution Exposure and Cardio- Respiratory Mortality: A Review. *Environ. Heal.* **2013**, *12* (1), 43.

(14) Understanding the health impact of air pollution in London https://www.kcl.ac.uk/lsm/research/divisions/aes/research/ERG/research-projects/HIAinLondonKingsReport14072015final.pdf.

(15) Ahn, M. W.; Park, K. S.; Heo, J. H.; Park, J. G.; Kim, D. W.; Choi, K. J.; Lee, J. H.; Hong, S. H. Gas Sensing Properties of Defect-Controlled ZnO-Nanowire Gas Sensor. *Appl. Phys. Lett.* **2008**, *93* (26), 2006–2009.

(16) Jun, J. H.; Yun, J.; Cho, K.; Hwang, I. S.; Lee, J. H.; Kim, S. Necked ZnO Nanoparticle-Based NO_2 Sensors with High and Fast Response. *Sensors and Actuators B: Chem.* **2009**, *140* (2), 412–417.

(17) Forleo, A.; Francioso, L.; Capone, S.; Siciliano, P.; Lommens, P.; Hens, Z. Synthesis and Gas Sensing Properties of ZnO Quantum Dots. *Sensors and Actuators B: Chem.* **2010**, *146* (1), 111–115.

(18) Xu, J. Q.; Pan, Q. Y.; Shun, Y. A.; Tian, Z. Z. Grain Size Control and Gas Sensing Properties of ZnO Gas Sensor. *Sensors and Actuators B-Chemical* **2000**, *66*, 277–279.

(19) Huang, Z. M.; Zhang, Y. Z.; Kotaki, M.; Ramakrishna, S. A Review on Polymer Nanofibers by Electrospinning and Their Applications in Nanocomposites. *Compos. Sci. Technol.* **2003**, *63* (15), 2223–2253.

(20) Hohman, M. M.; Shin, M.; Rutledge, G.; Brenner, M. P. Electrospinning and Electrically Forced Jets. II. Applications. *Phys. Fluids* **2001**, *13* (8), 2221–2236.

(21) Yang, X.; Shao, C.; Guan, H.; Li, X.; Gong, J. Preparation and Characterization of ZnO Nanofibers by Using Electrospun PVA/Zinc Acetate Composite Fiber as Precursor. *Inorg. Chem. Commun.* **2004**, *7* (2), 176–178.

(22) Rafieipour, H.; Vaezi, M. R.; Kazemzadeh, A. Synthesis and Characterisation of Ceramic Core/Shell Nanofibres via Single Stage Co-Axial Electrospinning. *Micro Nano Lett.* **2016**, *11* (11), 707–711.

(23) Sun, Z.; Zussman, E.; Yarin, A. L.; Wendorff, J. H.; Greiner, A. Compound Core-Shell Polymer Nanofibers by Co-Electrospinning. *Adv. Mater.* **2003**, *15* (22), 1929–1932.

(24) Öztürk, S.; Kilinç, N.; Öztürk, Z. Z. Fabrication of ZnO Nanorods for NO_2 Sensor Applications: Effect of Dimensions and Electrode Position. *J. Alloys Compd.* **2013**, *581* (2), 196–201.

(25) Zhang, C.; Debliquy, M.; Liao, H. Deposition and Microstructure Characterization of Atmospheric Plasma-Sprayed ZnO Coatings for NO_2 Detection. *Appl. Surf. Sci.* **2010**, *256* (20), 5905–5910.

(26) Jones, G. A. C.; Xiong, G.; Anderson, D.; Jones, G. A. C.; Xiong, G.; Anderson, D. Fabrication of Nanoscale ZnO Field Effect Transistors Using the Functional Precursor Zinc Neodecanoate Directly as a Negative Electron Beam Lithography Resist Fabrication of Nanoscale ZnO Field Effect Transistors Using the Functional Precursor Zinc Neodec. *J. Vac. Sci. Technol. B* **2009**, *27* (6), 3164–3168.

(27) Chen, Y.; Hong, S.; Ko, H.; Nakajima, M.; Segawa, T. Y.; Chen, Y.; Hong, S.; Ko, H.; Nakajima, M.; Yao, T. Plasma-Assisted Molecular-Beam Epitaxy of ZnO Epilayers on Atomically Flat Substrates Plasma-Assisted Molecular-Beam Epitaxy of ZnO Epilayers on Atomically. *Appl. Phys. Lett.* **2005**, *76* (2), 245–247.

(28) Adamopoulos, G.; Bashir, A.; Gillin, W. P.; Georgakopoulos, S.; Shkunov, M.; Baklar, M. A.; Stingelin, N.; Bradley, D. D. C.; Anthopoulos, T. D. Structural and Electrical Characterization of ZnO Films Grown by Spray Pyrolysis and Their Application in Thin- Film Transistors. *Adv. Funct. Mater.* **2011**, *21*, 525–531.

(29) Kim, K.; Song, J.; Jung, H.; Kim, K.; Song, J.; Jung, H.; Park, S.; Lee, J. Magnetron Sputtering Photoluminescence and Heteroepitaxy of ZnO on Sapphire Substrate (0001) Grown by Rf Magnetron Sputtering *. *J. Vac. Sci. Technol. A* **2000**, *18* (6), 2864–2868.

(30) Calleja, J.; Cardona, M. Resonant Raman Scattering in ZnO. *Phys. Rev. B* **1977**, *16* (8), 3753–3761.

(31) Bandyopadhyay, S.; Paul, G. K.; Roy, R.; Sen, S. K.; Sen, S. Study of Structural and Electrical Properties of Grain-Boundary Modified ZnO Films Prepared by Sol–Gel Technique. *Mater. Chem. Phys.* **2002**, *74* (1), 83–91.

(32) Lee, H. U.; Ahn, K.; Lee, S. J.; Kim, J. P.; Kim, H. G.; Jeong, S. Y.; Cho, C. R. ZnO Nanobarbed Fibers: Fabrication, Sensing NO_2 Gas, and Their Sensing Mechanism. *Appl. Phys. Lett.* **2011**, *98* (19), 2014–2017.

(33) Butt, H.J.; Graf, K.; Kappl, M. *Physics and Chemistry of Interfaces*; p 180, 2003.

(34) Straumal, B. B.; Protasova, S. G.; Mazilkin, A. A.; Goering, E.; Schütz, G.; Straumal, P. B.; Baretzky, B. Ferromagnetic Behaviour of ZnO: The Role of Grain Boundaries. *Beilstein J. Nanotechnol.* **2016**, *7* (1), 1936–1947.